THE JOURNAL OF PHYSICAL CHEMISTRY B

pubs.acs.org/JPCB Article

Insight into Electron Transfer from a Redox Polymer to a Photoactive Protein

Rafał Białek,* Kalyani Thakur, Adrian Ruff, Michael R. Jones, Wolfgang Schuhmann, Charusheela Ramanan, and Krzysztof Gibasiewicz*

Cite This: *J. Phys. Chem. B* 2020, 124, 11123–11132

Read Online

ACCESS | Metrics & More | Article Recommendations | Supporting Information

ABSTRACT: Biohybrid photoelectrochemical systems in photovoltaic or biosensor applications have gained considerable attention in recent years. While the photoactive proteins engaged in such systems usually maintain an internal charge separation quantum yield of nearly 100%, the subsequent steps of electron and hole transfer beyond the protein often limit the overall system efficiency and their kinetics remain largely uncharacterized. To reveal the dynamics of one of such charge-transfer reactions, we report on the reduction of *Rhodobacter sphaeroides* reaction centers (RCs) by Os-complex-modified redox polymers (P-Os) characterized using transient absorption spectroscopy. RCs and P-Os were mixed in buffered solution in different molar ratios in the presence of a water-soluble quinone as an electron acceptor. Electron transfer from P-Os to the photoexcited RCs could be described by a three-exponential function, the fastest lifetime of which was on the order of a few microseconds, which is a few orders of magnitude faster than the internal charge recombination of RCs with fully separated charge. This was similar to the lifetime for the reduction of RCs by their natural electron donor, cytochrome c_2. The rate of electron donation increased with increasing ratio of polymer to protein concentrations. It is proposed that P-Os and RCs engage in electrostatic interactions to form complexes, the sizes of which depend on the polymer-to-protein ratio. Our findings throw light on the processes within hydrogel-based biophotovoltaic devices and will inform the future design of materials optimally suited for this application.

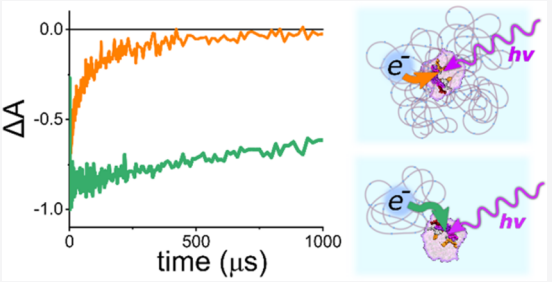

INTRODUCTION

Research into biohybrid solar energy conversion devices has expanded significantly over the past couple of decades, with a wide variety of device designs reported.[1−6] The biological component has usually been a photosynthetic protein such as photosystem I, photosystem II, or the reaction center (RC) from a purple photosynthetic bacterium; however, recently, there has been an increase in the usage of whole living organisms such as cyanobacteria immobilized directly on electrodes.[5] A wide variety of nonbiological components have been used as electrode substrates and electron acceptors or donors, including inorganic semiconductors, metals,[7,8] conductive polymers, and redox polymers. In addition to their sustainability, natural photosystems are attractive materials for solar energy conversion because of the very high quantum yields (event per photon absorbed) of both excitation energy transfer among their light-harvesting pigments and photochemical charge separation within the RC component. The benefit of high yield of charge separation is sustained by the rapid reduction of the redox center carrying the electron hole by an external donor, preventing wasteful charge recombination within the RC.[9]

A photoprotein that has been used extensively for the fabrication of biohybrid electrodes and devices is the RC from the purple bacterium *Rhodobacter sphaeroides*. This relatively simple RC conducts charge separation with a quantum yield of nearly 100%.[10] This functionality is provided by a set of cofactors buried inside an amino acid scaffold, namely, four bacteriochlorophylls (BChl; two of them are coupled in a so-called special pair and form the primary electron donor (P) and two are accessory BChls, B_A and B_B), two bacteriopheophytins (BPhe; H_A and H_B), two quinones (Q_A and Q_B), and one carotenoid (Car; see Figure 1A).[11] The absorption spectrum of the RC is characterized by bands that are attributed to different chromophores (Figure 1B). This allows for distinct spectral signatures in transient absorption (TA) spectroscopy, facilitating the analysis of photophysical pathways. The chromophores form two quasi-symmetric branches (A and B), but only one (branch A) is active in an electron-transfer process (Figure 1A). After light absorption, the excitation energy within the RCs is typically transferred to P,

Received: September 24, 2020
Revised: November 10, 2020
Published: November 25, 2020

https://dx.doi.org/10.1021/acs.jpcb.0c08714
J. Phys. Chem. B 2020, 124, 11123−11132

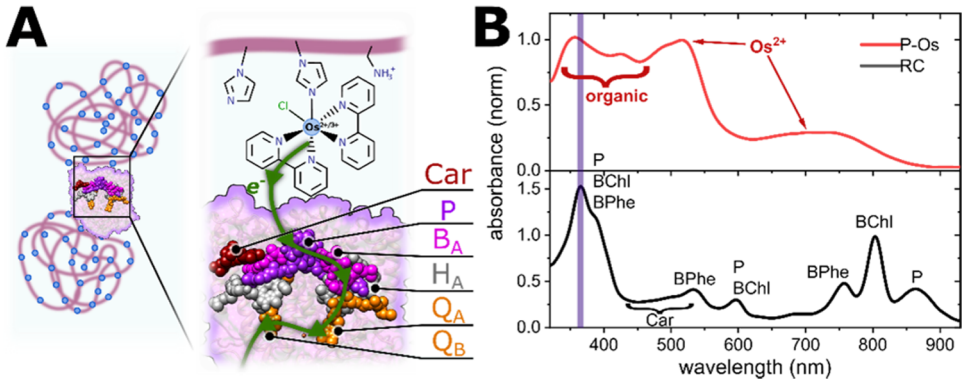

Figure 1. (A) Schematic of a possible complex of an RC and P-Os chains with an electron flow pathway. Os complexes are marked as blue dots in the zoomed-out view. (B) Steady-state absorption spectra of P-Os and RCs in a solution with band attributions. The 365 nm excitation wavelength is marked by a purple line.

forming the excited state P*. This triggers charge separation, resulting in the state $P^+H_A^-$. In this situation, the next step depends on the state of RCs, described in the literature as "open" or "closed".[12] Open RCs are those with all cofactors in their neutral state and thus able to conduct charge through the protein. In closed RCs, the electron transfer is blocked beyond H_A, either by reduction of Q_A or its removal. In the closed state, the only possibility for the separated charges on P^+ and H_A^- is to recombine. Usually, they relax back to the ground state of P, but there is also a low probability that a triplet excited state (^TP) can be formed (with a 15% yield in wild-type purified RCs[13−15]), leading finally to the formation and decay of a ^TCar state. On the other hand, in open RCs, the electron from H_A^- is transferred to Q_A within ∼200 ps, resulting in the $P^+Q_A^-$ state (which can recombine to the ground neutral state PQ_A within ∼100 ms), and next from Q_A^- to Q_B within ∼100−1000 μs, resulting in the $P^+Q_B^-$ state (which can recombine to the state PQ_B within ∼1 s). If the Q_B site is not occupied by a quinone in the purified RC, the final charge-separated state is $P^+Q_A^-$.[12,16]

The converted energy made available to *Rba. sphaeroides* through highly quantum-efficient charge separation within its RCs is secured by transferring the separated electron and hole to external acceptors and donors before they can recombine. The reduced quinone dissociates from the Q_B pocket in RC and is replaced by an oxidized quinone from an intramembrane pool, while the electron hole is transferred from P^+ to a water-soluble cytochrome c_2 (cyt c_2). This latter reaction is possible due to the formation of a transient complex between an RC and cyt c_2 mediated largely by electrostatic interactions.[17,18] Within this complex, cyt c_2 is oxidized on a ∼1 μs time scale.[19−23] This is several orders of magnitude faster than internal $P^+(Q_AQ_B)^-$ charge recombination in open RCs (0.1−1 s), stabilizing a high yield of charge separation.

Although a great deal is known about the kinetics, energetics, and structural bases of individual steps of charge separation and stabilization in *Rba. sphaeroides* RCs in solution, native membranes, and cells, very little detail is known about how these proteins operate on electrodes or in device settings. In general, only macroscopic parameters such as photocurrents and photovoltages have tended to be reported for RC biohybrid systems,[1,2,24] and to date, only a few attempts have been made to model the electron-transfer mechanism in such devices.[25−27] Precise modeling requires knowledge of the various parameters of the system, some of which can be accessed by employing electrochemical[24] or steady-state spectroelectrochemical[28] methods. However, the electron-transfer rate between the protein and the immediate external donor or acceptor has not yet been studied in detail. Transient absorption (TA) spectroscopy is the ideal tool for characterizing the rates of photoinduced electron-transfer reactions and has already been extensively used for the study of photoinduced charge separation and recombination dynamics in photosynthetic systems as well as in synthetic materials for solar energy conversion.[29−35]

Os-complex-modified redox polymers (P-Os) have been found to effectively wire photoactive proteins such as photosystem I,[36−38] photosystem II,[36,39−41] and *Rba. sphaeroides* RCs[28] to electrode surfaces. An efficient electron transfer within these systems is possible due to the proper redox potential of the P-Os. Moreover, when the protein is immobilized in the polymer matrix it can stabilize the protein complex and enhance its lifetime.[39,40] An intimate contact between the oppositely charged proteins and polymers can be achieved using charged polymer matrices, favoring a good electron exchange due to short electron pathways between an enzyme and a redox polymer.[42−44] Moreover, in addition to ensuring a good interaction with the enzyme, the positively or negatively charged groups within the redox polymer enable good water solubility and a high concentration of freely diffusing polymer chains in an aqueous media. This effect is used for the production of redox polymer-based aqueous flow batteries with high charge densities.[45] In this work, we have used a polymer with a mainly positive charge at pH 8 (see Figure 1A), which in principle is well suited to interaction with mainly negatively charged RCs. Moreover, Os-complex-modified redox polymers show absorption properties that are outside the main absorption region of the *Rba. sphaeroides* RC, and thus, they can be distinguished spectroscopically (Sokol et al., 2018; Figure 1B).

A combination of the P-Os polymer and *Rba. sphaeroides* RCs in a biophotoelectrode architecture has already been shown to give a relatively high internal quantum efficiency (∼50%) of photon to electron conversion.[28] This number implies a very good electrical contact between the P-Os and RCs immobilized inside this polymer matrix. For the present contribution, the dynamics and mechanism of the electron transfer between P-Os and bacterial RCs that underlies the high observed efficiency are explored. Since transient optical signals from the thin layer of a biophotoelectrode are extremely

https://dx.doi.org/10.1021/acs.jpcb.0c08714
J. Phys. Chem. B 2020, 124, 11123−11132

Table 1. Sample Compositions

	final concentration				
sample (P-Os/RC)[a]	RCs (μM)	polymer chains (μM)	Os complexes (μM)	Q_0 (mM)	ascorbate (mM)
I (3.1:1)	1.52 ± 0.10	4.7 ± 0.7	141 ± 17	1.48	
II (1.23:1)	1.54 ± 0.10	1.9 ± 0.29	56 ± 7	1.48	
III (0.64:1)	1.55 ± 0.10	0.99 ± 0.15	29.4 ± 3.6	1.49	
IV (6.4:1)	0.75 ± 0.05	4.8 ± 0.7	142 ± 17	1.49	
V (1.25:1)	3.76 ± 0.25	4.7 ± 0.7	139 ± 17	1.51	
RCs only	3.43 ± 0.22				
RCs + ascorbate	4.54 ± 0.30				9.7
RCs + P-Os	2.28 ± 0.15	3.9 ± 0.6	115 ± 14		
RCs + PVI + Q_0	1.52 ± 0.10	?[b]		1.48	
P-Os only		5.3 ± 0.8	158 ± 19		
P-Os + Q_0	4.04 ± 0.26			1.50	
Q_0 only				1.53	

[a]Values in parentheses are the molar ratios of P-Os to RCs. [b]Unknown due to unknown polymer molecular weight.

low; instead, we have investigated mixtures of P-Os and RCs suspended in the solution. TA spectroscopy has been used to demonstrate effective electron transfer between RCs and P-Os in the solution, the kinetics of which depend strongly on the molar concentration ratio between the P-Os and RCs. Steady-state experiments have also been conducted to understand the nature of the interaction between the proteins and polymer chains at different molar ratios.

EXPERIMENTAL SECTION

Purification of RCs. His_{10}-tagged *Rba. sphaeroides* RCs were purified as described in detail previously[46,47] using *N,N*-dimethyldodecan-1-amine oxide (LDAO; Sigma-Aldrich) as the solubilizing detergent and a combination of nickel affinity chromatography and size exclusion chromatography. Purified RCs were stored at −60 °C in 20 mM Tris (pH 8.0)/0.1% LDAO.

Polymer Synthesis. Syntheses of positively charged redox-silent polymer poly(vinyl imidazole-*co*-trimethyl aminoethyl methacrylate) (dubbed PVI; see Figure S1) and Os-complex-based redox polymer poly(vinyl imidazole-*co*-ally amine)-$[Os(II)(bpy)_2Cl]^+$ (dubbed P-Os) were as described previously.[48,49]

Solution Preparation. Samples for TA measurements were prepared in a quartz cuvette with a 2 mm optical path length (Gallab) from stock solutions diluted in 20 mM Tris (pH 8.0)/0.1% LDAO directly prior to the TA experiment. Stock solutions used were 10.0 ± 0.8 mg/mL polymer (either P-Os or PVI), 20.9 ± 1.4 mg/mL RCs, 15 mM 2,3-dimethoxy-5-methyl-*p*-benzoquinone (Q_0; Sigma-Aldrich), and 1 M sodium ascorbate (Sigma-Aldrich). Five experimental samples (named I−V) were prepared from stock solutions of RCs, P-Os, and Q_0, along with several control samples, as detailed in Table 1. Where present, the concentration of Q_0 was kept constant at around 1.5 mM to enable efficient electron acceptance from RCs.[28] More detailed information on the sample composition and preparation is given in Section S2 of the SI.

Solutions for steady-state experiments with centrifugation were prepared as for samples *I*−*V* for TA measurements but without Q_0 (the same amount of pure H_2O was used instead).

Steady-State Experiments. Steady-state absorption measurements were conducted using a Jasco V-770 spectrophotometer with an integrating sphere (ILN-925) in the same cuvette as used for TA measurements. Centrifugation was performed in 1.5 mL Eppendorf tubes in an Eppendorf MiniSpin centrifuge at 8000 rpm for 10 min. Absorbance spectra of polymer/protein mixtures were fitted with the sum of spectra of the P-Os and RC components with correction for scattering[50] to deconvolve their contribution using a script written in Python using the scipy.optimize module.[51]

Transient Absorption. TA experiments were conducted using the EOS extension in a Helios Fire pump-probe apparatus (Ultrafast Systems), paired with a regeneratively amplified 1030 nm laser (Light Conversion, Pharos, 200 fs). The effective laser repetition rate was set via an internal pulse picker. The pump (photoexcitation) pulse was generated with an optical parametric amplifier (Light Conversion, Orpheus-F). The broadband probe light was generated via a photonic crystal fiber (instrument response function (IRF) <1 ns). The parameters were as follows (if not stated otherwise): excitation wavelength, 365 nm; repetition rate, 100 Hz (and thus the time window ∼10 ms), and the excitation energy per pulse was 0.35 μJ (see Figure S6 for the amplitude vs excitation energy plot). Sample solutions were stirred with a magnetic stir bar at the slowest possible speed to provide a fresh sample between laser pulses.

The raw absorbance change data were fitted using Glotaran software for global analysis.[52,53] The resulting fitting function was the following

$$\Delta A(\lambda, t) = \sum_{i=1}^{n} A_i(\lambda)\, e^{-t/\tau_i} \quad (1)$$

where $\Delta A(\lambda, t)$ is the fit of absorbance change at wavelength λ and time t, $A_i(\lambda)$ is the ith preexponential factor, τ_i is the ith lifetime component, and n is the number of exponential components. Thus, for each wavelength, the absorbance change kinetics were fitted with the sum of exponential decay functions, but the lifetimes were shared among all wavelengths. The analysis yielded a set of spectra of preexponential factors, $A_i(\lambda)$, associated with particular lifetimes. These spectra are referred to as decay-associated difference spectra (DADS).

RESULTS AND DISCUSSION

Evidence of Electron Transfer from the Polymer to Protein in Solution. The application of TA spectroscopy on a millisecond time scale to RCs in buffer without any additional components produced a P^+/P difference spectrum.

https://dx.doi.org/10.1021/acs.jpcb.0c08714
J. Phys. Chem. B 2020, 124, 11123−11132

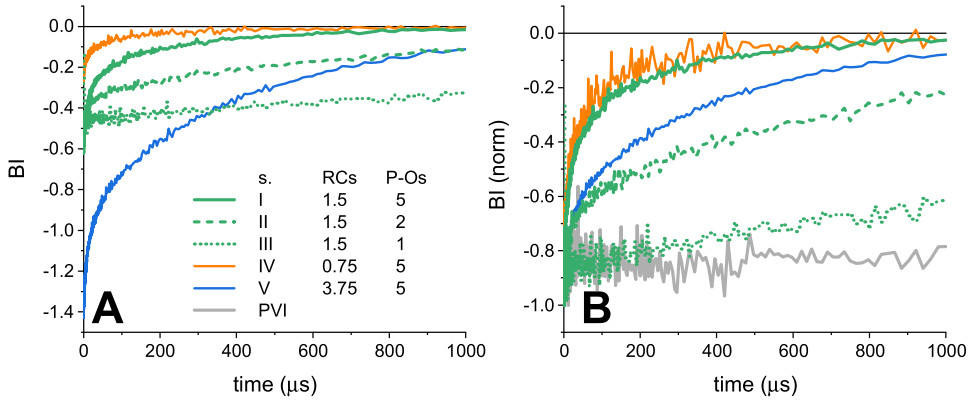

Figure 2. (A) Band integral (BI) kinetics for the first 1 ms. Band integrals were constructed in the 830−950 nm range. (B) Same data normalized to −1 at minimum. Values in the legend represent rounded molar concentrations of RCs and P-Os (in μM unit; for exact values, see Table 1). Kinetics reveal rates of electron transfer from the polymer to the protein.

This had distinctive negative signals at around 870 and 600 nm attributable to the bleach of P ground-state absorbance and electrochromic blue and red shifts at around 800 and 760 nm coming from the accessory BChls and BPhes, respectively (Figure S2). The apparent shortening of the lifetime of the P^+ state obtained in this paper (11 ms) in comparison to lifetimes from the literature (~100 ms in the absence and ~1 s in the presence of Q_B[12]) was likely due to the depletion of RCs in the charge-separated state in the small focal volume of the laser beam. This was caused by stirring that moved photoexcited proteins out of the focal volume (see Figure S3 for comparison).

The addition of sodium ascorbate to the solution of RCs causes their closing by the formation of reduced Q_A (Q_A^-). The occurrence of this was evidenced (Figure S5) by the appearance of faster decay components attributable to $P^+H_A^-$ charge recombination (on the order of ~10 ns[54,55]) and ^{T}Car formation and decay (nanoseconds and microseconds, respectively[56,57]).

The addition of P-Os (reduced form, Os(II)-species) to the solution of RCs rather than ascorbate resulted in spectra and lifetimes (Figure S6) that were similar to those obtained with ascorbate (Figure S5). As P-Os alone did not show any TA signals in the studied time range (not shown), we conclude that the P-Os is able to reduce P^+ in the RC, creating a closed state. This observation is novel, as so far this kind of process was observed only in RC- or photosystem I-based biohybrid electrodes but not in a mixture of proteins and polymers in solution.[28,36−38] It validates that P-Os and RCs are properly paired for electron transfer between them, suggesting good pairing also while immobilized on the electrode. However, it is important to note that immobilization can change the properties of the material, such as redox potentials;[28] thus, in situ methods should be used on biohybrid devices for final verification. The fully reduced initial state of the P-Os and a concentration of species were favorable for the reduction of RCs by P-Os (there are at least 20 times more Os complexes than RCs in solutions; Table S3). However, this reduction leads to the closing of RCs prior to the TA experiment so it is impossible to measure its rate in the described type of experiment. An equivalent experiment with the PVI backbone polymer, which acts as a redox-silent mimic for P-Os, did not produce nanosecond/microsecond decay components (Figure S4) and showed only RC charge recombination occurring on the millisecond time scale as in the absence of ascorbate (Figure S2).

To measure the kinetics of electron transfer from the P-Os to P^+, it was necessary to keep RCs in their open state to get a long enough lifetime of the P^+ state (~100 ms in open RCs vs ~10 ns in closed RCs). To keep RCs in their open state, the excess electrons have to be taken away from Q_A^- by adding an external electron acceptor. The addition of water-soluble ubiquinone (Q_0) allowed the following reaction to be monitored

$$\text{P-Os(II)} + PQ_A + Q_0(\text{ox}) \xrightarrow{\text{laser pulse}} \text{P-Os(II)} + P^+Q_A^- + Q_0(\text{ox}) \rightarrow \text{P-Os(III)} + PQ_A + Q_0(\text{red})$$

The water-soluble Q_0 has already proven its usefulness in biohybrid devices as an electron acceptor from the Q-side of RCs, replacing naturally functioning ubiquinone-10 within the membrane.[58] Its usefulness comes from the fact that quinone reduction is coupled with protonation; thus, its reaction with a bare electrode is relatively inefficient, while its interaction with RCs is fast due to its specific (enzymatic) nature.[59]

The presence of Q_0 in the solution alone or with the P-Os did not give any TA signals in the studied time range.

Kinetics of Electron Transfer from the Polymer to Protein. Mixtures of RCs, P-Os, and Q_0 were prepared at five different molar ratios of P-Os/RC (Table 1). For all samples, the difference spectrum just after laser excitation resembled that of oxidized P (in the charge-separated state $P^+(Q_AQ_B)^-$; Figure S2) and the spectrum then evolved over time. To observe the kinetics of the P^+ decay, band integrals (kinetics of the raw TA signal integrated over selected wavelength range) were calculated in the range 830−950 nm, corresponding to the bleach of P ground-state absorption (Figure 2). Band integrals (BIs) were used instead of single wavelength kinetics to increase the signal-to-noise ratio. For data that were not normalized (Figure 2A), the starting amplitude of the signal depended on the concentration of RCs, while the shape of the decay curve also depended on the concentration of P-Os. After normalizing to the initial signal amplitude (Figure 2B), it was evident that for all concentrations of P-Os the decay was faster than that for a reference sample without P-Os electron donor. Moreover, a faster rate of decay of P^+ exhibited a direct correlation with a higher concentration of P-Os and an

https://dx.doi.org/10.1021/acs.jpcb.0c08714
J. Phys. Chem. B 2020, 124, 11123−11132

opposite correlation with the increasing concentration of RCs, suggesting that P^+ decay was caused due to its reduction by the P-Os.

TA spectra averaged over a 4−6 ms delay revealed which species remained at the end of the period monitored (Figure 3,

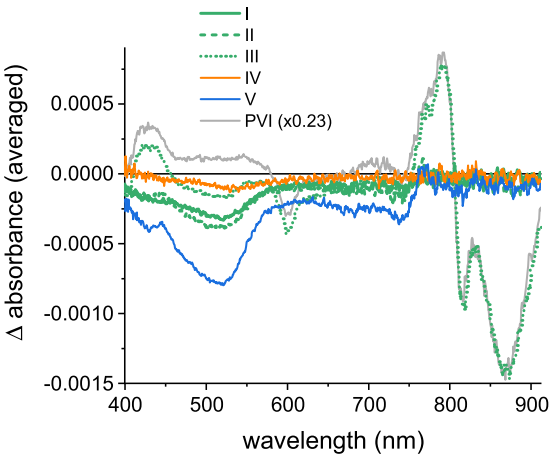

Figure 3. Averages of transient absorption spectra at delay times of 4−6 ms. The averaged spectrum for the PVI sample (redox-silent polymer) was scaled to match the sample III spectrum in the long-wavelength region to show its polymer and RC (P/P^+) contributions in the latter spectrum. All of the remaining spectra are dominated by the signal from the polymer. Averaging over the 4−6 ms window was performed to improve the signal-to-noise ratio.

spectra at other delays are shown in Figures S8−S12). For most samples, the main features were negative signals centered at ∼520 and ∼740 nm. These can be attributed to bleaches arising from the oxidation of Os(II) to Os(III) in the P-Os.[28] The exception was sample III, which had the lowest concentration of P-Os and the lowest ratio of Os complexes per RC. The spectrum of this sample showed a mixture of RC and P-Os signals (compare it to pure RC signal in the sample with PVI, Figure 3). The data confirmed the hypothesis that there is electron transfer from the Os complexes in the polymer to P^+ in the RCs, showing that nearly 100% of photoexcited RCs, which were in an open state before the excitation flash, could be reduced provided that the relative concentration of Os complexes was sufficiently high. If it was not, then P^+ reduction was inefficient, either because the electron transfer was not that efficient under these conditions or it was slower than the time window. Under the conditions of the TA experiment, the signal completely vanished within 10 ms due to the excited species gradually escaping from the observed focal volume of the sample, hampering the resolution of slow reduction processes.

Kinetic Phases of Electron Transfer from the Polymer to Protein. Global analysis produced sets of DADS and associated lifetimes. Shapes of DADS were similar for samples I, II, IV, and V, differing mainly in amplitude. A representative set for sample I are shown in Figure 4, and the remainder is shown in Figures S13−S16. The best fit was obtained from a four-exponential model with all lifetimes set to be free. The three fastest DADSs were similar in shape to one another and corresponded well to the P/P^+ difference spectrum.[28] The slowest DADS represented the escape of the excited sample from the laser focal volume rather than the real decay of an observed state. In general, this escape is not a simple

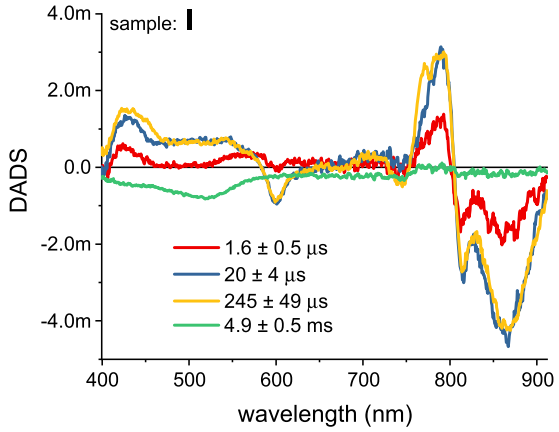

Figure 4. DADS for sample I and associated lifetimes. Individual spectra contain contributions from the protein and/or polymer.

exponential function but a single exponential was sufficient to fit the data at the present level of noise. Thus, the slowest component can be treated as a nondecaying signal left after former reactions and showed mostly photobleaching of ground-state P-Os absorbance, suggesting that the three faster DADS should include features of the P-Os oxidation process. For sample III (Figure S14), this fitting procedure did not give a fully acceptable result, as the two slowest components clearly compensated one another. However, when fewer exponential components were used, the fitting seemed to omit the P-Os signal completely (not shown). The compensation for the two slowest DADS suggests that the lifetime of the electron transfer, in this case, was very similar to that of the photoexcited part of the sample escaping the focal volume (i.e., ∼4−5 ms). Thus, for this sample, the amplitudes of the two slowest DADS were not suitable for further analysis.

To look for a contribution of P-Os oxidation in the first three DADS, the P/P^+ differential spectrum in the form of the DADS from the RC-only sample (Figure S2) was subtracted from all of them. This P/P^+ differential spectrum was scaled in amplitude such that the signal in the resulting difference spectra in the range 780−900 nm was as close to zero as possible (for verification of this, see Figures S21−S25). It was achieved using a script written in Python using the scipy.optimize module.[51] The resulting "ΔDADS" for sample I is shown in Figure 5, and for the remainder, see Figures S17−S20. The fastest ΔDADS had a maximum at around 600 nm and was slightly negative at 500 nm. It resembled the shape of the difference spectrum expected for Car triplet decay (see Figure S5 for comparison) with the possible addition of some oxidation of P-Os, causing a shallowing of the ∼500 nm valley visible in Figure S5. The reason why a ^{T}Car state was observed is likely to be because the added Q_0 might not be fully efficient in accepting electrons from the Q-side of RCs between laser shots, leading to the formation of ^{T}Car in closed RCs in the state PQ_A^-. Moreover, it is conceivable that access of Q_0 to the Q-side of the protein in some RCs may have been locked by the adsorbed polymer (see below). Accordingly, the fastest ΔDADS is attributed to a mixture of ^{T}Car decay (expected lifetime ∼2.5−4 μs)[56,57] and P-Os → P^+ electron transfer. However, the main amplitude of this decay lies in the >750 nm region, where the signal comes almost exclusively from P/P^+, and thus, P-Os → P^+ electron transfer has the dominating contribution to this lifetime. Taking into account equivalent details for the remaining samples (Figures S17−S20), it is

https://dx.doi.org/10.1021/acs.jpcb.0c08714
J. Phys. Chem. B 2020, 124, 11123−11132

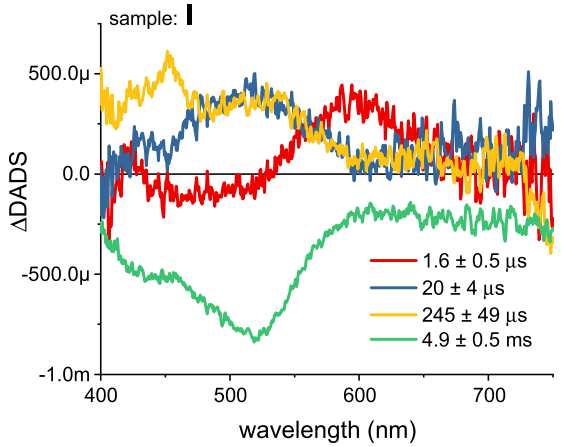

Figure 5. ΔDADS for sample I obtained by subtracting RC contributions from the DADS in Figure 4. Subtraction was performed primarily to reveal the formation of the oxidized form of the polymer.

concluded that the fastest electron transfer from P-Os to P^+ occurred on the time scale of 0.5−5 μs. The next two ΔDADS with lifetimes of 20 and 245 μs in Figure 5 had a prominent positive amplitude at around 515 nm attributable to the formation of the oxidized state of P-Os. The slowest ΔDADS, attributed to the sample escaping the focal volume, matched the spectral signature of loss of oxidized P-Os, also consistent with electron transfer from P-Os to P^+, occurring over a microsecond time scale.

Mechanism of Electron Transfer from the Polymer to Protein. The sample compositions allowed exploration of the dependence of the electron-transfer rates on the concentrations of both RCs and P-Os (Figure 6). At a fixed concentration of P-Os (Figure 6A), a higher concentration of RCs resulted in a lower rate constant (slower electron transfer). At a fixed concentration of RCs (Figure 6B), a higher concentration of P-Os gives an opposite effect with a higher rate constant (faster electron transfer). As shown in Figure 6C, the rate of all three components of the electron transfer accelerated as the ratio of P-Os/RC increased.

Analysis of the amplitudes associated with the DADS (Figure 7A) showed that there was an increase in the relative contribution of the two faster components with increasing P-Os/RCs molar ratio, thus accelerating the overall process. There are two possible descriptions of this behavior.

Collisional Model. The simplest description of the electron-transfer reaction would be collisional interactions of RCs with aggregates of P-Os of different sizes or structures, producing different electron-transfer rates. For this type of interaction, the kinetics of electron transfer would be governed by eq 2

$$\frac{\mathrm{d}[\mathrm{P}]}{\mathrm{d}t} = k[\mathrm{P} - \mathrm{Os(II)}][\mathrm{P}^+] \tag{2}$$

During the reaction, the concentration of P-Os(II) remained almost constant (the amplitude of the slowest DADS was no more than 0.5% of the amplitude of the steady-state absorbance of P-Os). Thus, this reaction can be treated as a pseudo-first-order with the apparent first-order rate constant (k_{app}) given by eq 3.

$$k_{app} = k[\mathrm{P} - \mathrm{Os(II)}] \tag{3}$$

Although this would explain the dependence of the electron-transfer rate on the concentration of P-Os, it does not explain its dependence on the concentration of RCs. This indicates that there must be interactions other than collisions occurring, such as the creation of quasi-stable complexes between RCs and P-Os in solution.

Complexing Model. Electron donation to P^+ in RCs in solution has been studied in depth for the natural electron donor, cyt c_2, and has been reported to be biexponential.[19−23,60] To account for this, a model incorporating the creation of semistable complexes has been proposed.[19,22] The faster component (lifetime ∼1 μs) was attributed to the electron-transfer rate within an RC/cyt c_2 complex, while the slower component was attributed to the diffusion-limited creation of complexes convolved with direct electron transfer. The finding that the faster component of reduction of P^+ by cyt c_2 was independent of concentration is in contrast with our findings for the RC/P-Os system. Moreover, it was reported that the rate of P^+ reduction increased with increasing cyt c_2 concentration and increased with the concentration of RCs, which is opposite to the effect observed in the present paper.[22,23,60] Thus, the model constructed for cyt c_2 cannot be

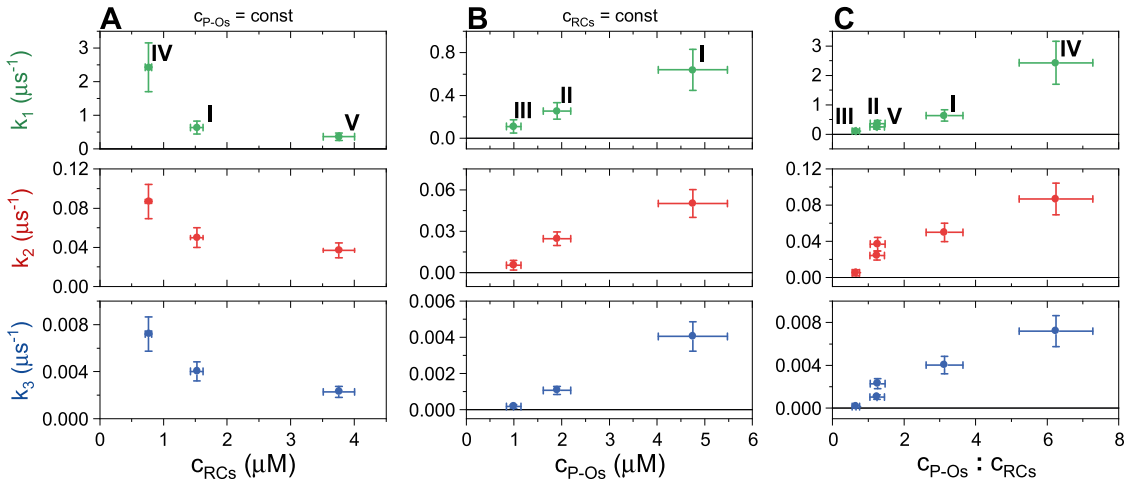

Figure 6. Dependence of electron-transfer rate constants (reciprocals of lifetimes) on (A) concentrations of RCs for a constant concentration of P-Os, (B) concentration of P-Os for a constant concentration of RCs, and (C) molar ratio of P-Os chains to RCs. Note that all rate constants increase with increasing ratio of the polymer to protein concentrations.

https://dx.doi.org/10.1021/acs.jpcb.0c08714
J. Phys. Chem. B 2020, 124, 11123−11132

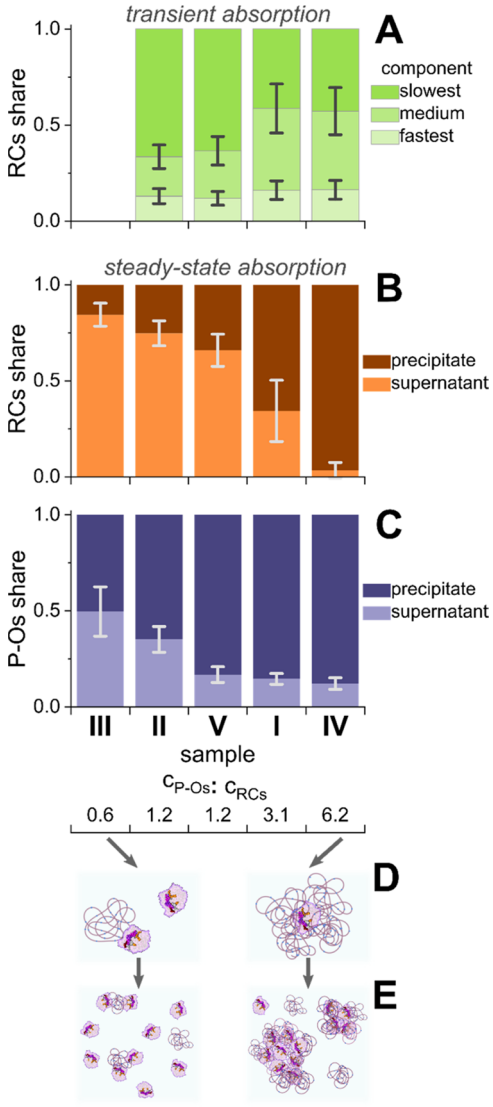

Figure 7. (A) Relative contributions of the three DADS components from TA experiments to the overall process as a function of the molar ratio of P-Os/RC. (B) Relative amount of RCs in the precipitate and supernatant, determined from steady-state absorption measurements on centrifuged samples, as a function of the molar ratio of P-Os/RC. (C). Relative amount of P-Os in the precipitate and supernatant, determined from steady-state absorption measurements on centrifuged samples, as a function of the molar ratio of P-Os/RC. (D, E) Schemes of complex formation for lower and upper limits of polymer-to-protein ratios (see the text for details). Note that the higher the polymer-to-protein ratio, the stronger the effect of complexes formation (B–E).

directly used in the system with P-Os and RCs. However, it is interesting to note that the fastest lifetime for electron transfer between RCs and P-Os is of the same order as that for RCs and cyt c_2. This informed the hypothesis that RCs create complexes with P-Os and at least some of them are as efficient in electron donation as natural cytochrome c_2. The similar behavior of all lifetimes (Figure 6) suggests that they arise from complexes with different compositions that produce different electron-transfer rates.

To examine whether complexes form between RCs and P-Os, mixtures were centrifuged at 8000 rpm for 10 min, a treatment that resulted in part of both the RC and P-Os population being spun down from the solution. This indicated that, in all samples, there had been the formation of complexes large enough to be centrifuged out. The fraction of both RCs and P-Os to be pelleted increased as the molar ratio of P-Os/RC increased (Figure 7B,C), suggesting that more or larger complexes had been formed. The finding that higher concentration ratios also produced a decrease in the contribution of the slowest component of the electron transfer (Figure 7A) suggests that such conditions produce more complexes with a favorable orientation of P-Os and RCs.

There remains a question about the nature of complexes formed between RCs and the P-Os. The interaction between the RC and cyt c_2 is primarily electrostatic with the cytochrome being positively charged and its binding site on the RC negatively charged[17,18] under native pH conditions (pH 8; Figure 8). The charge of the P-Os is determined by the states

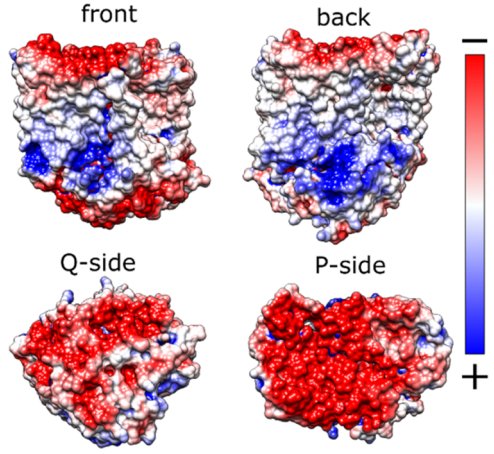

Figure 8. Distribution of the surface charge on RCs at pH 8.0. The simulation was done using PDB2PQR and APBS software with the 1PCR structure from PDB[61] at default settings.[62,63] Negatively charged surfaces preferentially interact with the polymer.

of its component groups in its structure (Figure 1A). Os complexes remain positively charged independently of the pH of the solution. However, it has been reported that at pH 8 most of the imidazole and primary amino groups remain in an unprotonated, uncharged state.[37] Thus, P-Os is mainly positively charged at pH 8 due to the presence of positively charged Os complexes. It is known that P-Os has a tendency to form loosely bound agglomerates in solution at pH 6.5, with the smallest particles being on the order of 16 nm in radius.[40] It was also reported that for pH ≥7, films made of P-Os collapse.[37] Thus, in the conditions studied in this paper, P-Os entities exist most probably as particles with a hydrodynamic radius of no longer than 16 nm, or loosely bound agglomerates of such particles, and are positively charged. This would be consistent with net anionic RCs and cationic P-Os particles forming complexes through electrostatic interactions.

For cyt c_2, an additional factor contributing to the formation of a complex with RCs in the proper mutual orientation is the shape of the protein. The cytochrome binds in a highly specific manner to a site on the periplasmic side (P-side) of the RC that has a complementary shape and charge. For a polymer, this shape factor is more random, and it is conceivable that P-Os could attach to any part of the RC protein on either the P-side or Q-side that has a suitable surface charge (Figure 8). The most optimal interaction would be one where a P-Os

https://dx.doi.org/10.1021/acs.jpcb.0c08714
J. Phys. Chem. B 2020, 124, 11123−11132

attached to the P-side of the RC with one of its Os complexes as close as possible to the P bacteriochlorophylls on the surface of the protein. The least optimal attachment would be at the Q-side, producing very slow electron transfer that would compete poorly with charge recombination internal to the RC. In addition, binding of P-Os to the Q-side could conceivably hamper access of the Q_0 electron acceptor to the Q_B pocket. Enhanced recombination would be observable on the studied time scale as triplet state formation (see section Kinetic Phases of Electron Transfer from the Polymer to Protein). When the polymer-to-protein molar ratio is close to or even smaller than 1:1, the electron transfer is the slowest (see Figure 6C). This ratio means that there is one polymer chain per protein on average and, as it can be attached at random sites of RCs, the observed electron transfer might be expected to be relatively slow. For higher polymer-to-protein ratios, there might be more than one polymer chain attached to the RC, increasing the probability of one occupying an optimal position that leads to better wiring between the polymer and RC and thus increases the observed electron-transfer rate. This scenario is depicted schematically in Figure 7D. On the other hand, we speculate that with increasing number of polymer chains per protein, the probability of formation of large aggregates increases, with polymers acting like an electrostatic "glue" (Figure 7E). This would explain why in centrifugation experiments the amount of precipitate containing both polymers and proteins increases with increasing molar ratio of P-Os/RC (Figure 7B,C).

Mechanistic Significance and Conclusions. The TA data demonstrate that P-Os and RCs interact strongly in solution despite being sparsely dispersed compared to those in a hydrogel on an electrode surface. The P-Os polymer is capable of reducing photoinduced P^+ with time constants distributed over a range of a few microseconds to around 1 ms. The fastest electron transfer from P-Os to P^+ occurred on the time scale of 0.5−5 μs, values that are similar to the ∼1 μs lifetime of the natural electron transfer between complexed RC and cyt c_2.[19−23] This demonstrates that P-Os in the proper conformation can perform as efficiently as a natural donor in terms of the electron-transfer rate. The exact value of the time constant depended on the concentration ratio between P-Os and RCs, being the fastest for the highest ratios. The data allowed derivation of a hypothesis that P-Os and RCs create complexes in solution through electrostatic interactions, and it is suggested that the lifetime of electron transfer for a single complex depends mostly on its detailed conformation and, in particular, precisely where on the protein surface the polymer binds.

Irrespective of sample composition, all three lifetimes for electron transfer from the polymer to protein were orders of magnitude faster than naturally occurring charge recombination of the $P^+(Q_AQ_B)^-$ state (0.1−1 s), and so it was at least 100 times more probable for this electron transfer to occur rather than charge recombination. This promising finding is one of the explanations for the relatively high (∼50%) internal quantum efficiency of a biophotoelectrode consisting of RCs and P-Os reported previously.[28]

These results explain the relatively high efficiencies of photoelectrodes based on redox hydrogels and RCs in comparison to other architectures with RCs. They show that surface properties (e.g., electrostatic) that govern the interactions between natural and synthetic components in a biohybrid material are at least as important as the proper matching of redox levels. Moreover, the TA technique presented in this study may in principle be used to monitor electron-transfer rates in situ in an operational device. Such an approach enables a better understanding of the electron-transfer process by obtaining exact values of reaction rate constants, which are necessary for precise modeling and identifying possible bottlenecks limiting the performance of the devices.

■ ASSOCIATED CONTENT

Supporting Information

The Supporting Information is available free of charge at https://pubs.acs.org/doi/10.1021/acs.jpcb.0c08714.

Structure of the redox-silent polymer, detailed information on the sample preparation, reference experiments results, difference spectra at chosen delays, and global analysis results for samples omitted in the main text (PDF)

■ AUTHOR INFORMATION

Corresponding Authors

Rafał Białek − *Faculty of Physics, Adam Mickiewicz University, 61-614 Poznań, Poland;* orcid.org/0000-0002-4874-4637; Email: rafal.bialek@amu.edu.pl

Krzysztof Gibasiewicz − *Faculty of Physics, Adam Mickiewicz University, 61-614 Poznań, Poland;* orcid.org/0000-0003-1803-6282; Email: krzysztof.gibasiewicz@amu.edu.pl

Authors

Kalyani Thakur − *Max Planck Institute for Polymer Research, 55128 Mainz, Germany;* orcid.org/0000-0002-2374-2838

Adrian Ruff − *Analytical Chemistry Center for Electrochemical Sciences, Faculty of Biochemistry and Chemistry, Faculty of Biochemistry and Chemistry, Ruhr-University Bochum, D-44780 Bochum, Germany;* orcid.org/0000-0001-5659-8556

Michael R. Jones − *School of Biochemistry, Biomedical Sciences Building, University of Bristol, University Walk, Bristol BS8 1TD, U.K.;* orcid.org/0000-0002-8063-0744

Wolfgang Schuhmann − *Analytical Chemistry Center for Electrochemical Sciences, Faculty of Biochemistry and Chemistry, Faculty of Biochemistry and Chemistry, Ruhr-University Bochum, D-44780 Bochum, Germany;* orcid.org/0000-0003-2916-5223

Charusheela Ramanan − *Max Planck Institute for Polymer Research, 55128 Mainz, Germany;* orcid.org/0000-0001-8603-6853

Complete contact information is available at: https://pubs.acs.org/10.1021/acs.jpcb.0c08714

Notes

The authors declare no competing financial interest.

■ ACKNOWLEDGMENTS

R.B. acknowledges support from the Ministry of Science and Higher Education, Poland (project entitled: "Construction of solar cells based on purple bacteria reaction centers and polymer hydrogels" no. 0129/DIA/2016/45). K.G. acknowledges support from the National Science Center, Poland (project entitled "Bio-semiconductor hybrids for photovoltaic

cells" no. 2012/07/B/NZ1/02639). W.S. and A.R. thank the Deutsche Forschungsgemeinschaft (DFG) under Germany's Excellence Strategy EXC-2033 (project number 390677874) for financial support. MRJ acknowledges support from the BrisSynBio Synthetic Biology Research Center at the University of Bristol (BB/L01386X/1). The authors thank Dr. Sabine Alsaoub for the synthesis of the redox-silent polymer backbone.

■ ABBREVIATIONS USED

RC	reaction center
Rba	*Rhodobacter*
TA	transient absorption
P-Os	osmium-complex-modified redox polymer (poly(vinyl imidazole-co-allyl amine)-[$Os(bpy)_2Cl$]Cl with bpy = 2,2′ bipyridine)
PVI	redox-silent poly(vinyl imidazole)-based polymer
DADS	decay-associated difference spectrum/spectra

■ REFERENCES

(1) Ravi, S. K.; Tan, S. C. Progress and Perspectives in Exploiting Photosynthetic Biomolecules for Solar Energy Harnessing. *Energy Environ. Sci.* **2015**, *8*, 2551−2573.
(2) Friebe, V. M.; Frese, R. N. Photosynthetic Reaction Center-Based Biophotovoltaics. *Curr. Opin. Electrochem.* **2017**, *5*, 126−134.
(3) Milano, F.; Punzi, A.; Ragni, R.; Trotta, M.; Farinola, G. M. Photonics and Optoelectronics with Bacteria: Making Materials from Photosynthetic Microorganisms. *Adv. Funct. Mater.* **2019**, *29*, No. 1805521.
(4) Musazade, E.; Voloshin, R.; Brady, N.; Mondal, J.; Atashova, S.; Zharmukhamedov, S. K.; Huseynova, I.; Ramakrishna, S.; Najafpour, M. M.; Shen, J. R.; et al. Biohybrid Solar Cells: Fundamentals, Progress, and Challenges. *J. Photochem. Photobiol., C* **2018**, *35*, 134−156.
(5) Kornienko, N.; Zhang, J. Z.; Sakimoto, K. K.; Yang, P.; Reisner, E. Interfacing Nature's Catalytic Machinery with Synthetic Materials for Semi-Artificial Photosynthesis. *Nat. Nanotechnol.* **2018**, *13*, 890−899.
(6) Nagy, L.; Magyar, M.; Szabó, T.; Hajdu, K.; Giotta, L.; Dorogi, M.; Milano, F. Photosynthetic Machineries in Nano-Systems. *Curr. Protein Pept. Sci.* **2014**, *15*, 363.
(7) Friebe, V. M.; Delgado, J. D.; Swainsbury, D. J. K. K.; Gruber, J. M.; Chanaewa, A.; van Grondelle, R.; Von Hauff, E.; Millo, D.; Jones, M. R.; Frese, R. N. Plasmon-Enhanced Photocurrent of Photosynthetic Pigment Proteins on Nanoporous Silver. *Adv. Funct. Mater.* **2016**, *26*, 285−292.
(8) Kowalska, D.; Szalkowski, M.; Sulowska, K.; Buczynska, D.; Niedziolka-Jonsson, J.; Jonsson-Niedziolka, M.; Kargul, J.; Lokstein, H.; Mackowski, S. Silver Island Film for Enhancing Light Harvesting in Natural Photosynthetic Proteins. *Int. J. Mol. Sci.* **2020**, *21*, No. 2451.
(9) Blankenship, R. E. *Molecular Mechanisms of Photosynthesis*; Blackwell Science Ltd.: Oxford, U.K., 2002.
(10) Wraight, C. A.; Clayton, R. K. The Absolute Quantum Efficiency of Bacteriochlorophyll Photooxidation in Reaction Centres of Rhodopseudomonas Spheroides. *Biochim. Biophys. Acta, Bioenerg.* **1974**, *333*, 246−260.
(11) Allen, J. P.; Feher, G.; Yeates, T. O.; Komiya, H.; Rees, D. C. Structure of the Reaction Center from Rhodobacter Sphaeroides R-26: The Cofactors. *Proc. Natl. Acad. Sci. U.S.A.* **1987**, *84*, 5730−5734.
(12) Woodbury, N. W.; Allen, J. P. The Pathway, Kinetics and Thermodynamics of Electron Transfer in Wild Type and Mutant Reaction Centers of Purple Nonsulfur Bacteria. In *Anoxygenic Photosynthetic Bacteria*; Blankenship, R. E.; Madigan, M.; Bauer, C. E., Eds.; Kluwer Academic Publishers: Dordrecht, 1995; pp 527−557.
(13) Parson, W. W.; Cogdell, R. J. The Primary Photochemical Reaction of Bacterial Photosynthesis. *Biochim. Biophys. Acta, Rev. Bioenerg.* **1975**, *416*, 105−149.
(14) Michel-Beyerle, M. E.; Scheer, H.; Seidlitz, H.; Tempus, D. Magnetic Field Effect on Triplets and Radical Ions in Reaction Centers of Photosynthetic Bacteria. *FEBS Lett.* **1980**, *110*, 129−132.
(15) Schenck, C. C.; Blankenship, R. E.; Parson, W. W. Radical-Pair Decay Kinetics, Triplet Yields and Delayed Fluorescence from Bacterial Reaction Centers. *Biochim. Biophys. Acta, Bioenerg.* **1982**, *680*, 44−59.
(16) Okamura, M. Y.; Feher, G. Proton-Coupled Electron Transfer Reactions of QB in Reaction Centers from Photosynthetic Bacteria. In *Anoxygenic Photosynthetic Bacteria*; Blankenship, R. E.; Madigan, M.; Bauer, C., Eds.; Kluwer Academic Publishers: Dordrecht, 1995; pp 577−593.
(17) Tiede, D. M.; Vashishta, A. C.; Gunner, M. R. Electron-Transfer Kinetics and Electrostatic Properties of the Rhodobacter Sphaeroides Reaction Center and Soluble c-Cytochromes. *Biochemistry* **1993**, *32*, 4515−4531.
(18) Miyashita, O.; Onuchic, J. N.; Okamura, M. Y. Continuum Electrostatic Model for the Binding of Cytochrome C2 to the Photosynthetic Reaction Center from Rhodobacter Sphaeroides. *Biochemistry* **2003**, *42*, 11651−11660.
(19) Abresch, E. C.; Gong, X. M.; Paddock, M. L.; Okamura, M. Y. Electron Transfer from Cytochrome C2 to the Reaction Center: A Transition State Model for Ionic Strength Effects Due to Neutral Mutations. *Biochemistry* **2009**, *48*, 11390−11398.
(20) Overfield, R. E.; Wraight, C. A.; Devault, D. Microsecond Photooxidation Kinetics of Cytochrome C2 from Rhodopseudomonas Sphaeroides: In Vivo and Solution Studies. *FEBS Lett.* **1979**, *105*, 137−142.
(21) Tetreault, M.; Rongey, S. H.; Feher, G.; Okamura, M. Y. Interaction between Cytochrome C2 and the Photosynthetic Reaction Center from Rhodobacter Sphaeroides: Effects of Charge-Modifying Mutations on Binding and Electron Transfer. *Biochemistry* **2001**, *40*, 8452−8462.
(22) Farchaus, J. W.; Wachtveitl, J.; Mathis, P.; Oesterhelt, D. Tyrosine 162 of the Photosynthetic Reaction Center L-Subunit Plays a Critical Role in the Cytochrome C2 Mediated Rereduction of the Photooxidized Bacteriochlorophyll Dimer in Rhodobacter Sphaeroides. 1. Site-Directed Mutagenesis and Initial Characterization. *Biochemistry* **1993**, *32*, 10885−10893.
(23) Moser, C. C.; Dutton, P. L. Cytochrome c and C2Binding Dynamics and Electron Transfer with Photosynthetic Reaction Center Protein and Other Integral Membrane Redox Proteins. *Biochemistry* **1988**, *27*, 2450−2461.
(24) Plumeré, N.; Nowaczyk, M. M. Biophotoelectrochemistry of Photosynthetic Proteins. In *Advances in Biochemical Engineering/Biotechnology*; Springer, 2016; Vol. *123*, pp 127−141.
(25) Białek, R.; Swainsbury, D. J. K.; Wiesner, M.; Jones, M. R.; Gibasiewicz, K. Modelling of the Cathodic and Anodic Photocurrents from Rhodobacter Sphaeroides Reaction Centres Immobilized on Titanium Dioxide. *Photosynth. Res.* **2018**, *138*, 103−114.
(26) Buesen, D.; Hoefer, T.; Zhang, H.; Plumeré, N. A Kinetic Model for Redox-Active Film Based Biophotoelectrodes. *Faraday Discuss.* **2019**, *215*, 39−53.
(27) Milano, F.; Ciriaco, F.; Trotta, M.; Chirizzi, D.; De Leo, V.; Agostiano, A.; Valli, L.; Giotta, L.; Guascito, M. R. Design and Modelling of a Photo-Electrochemical Transduction System Based on Solubilized Photosynthetic Reaction Centres. *Electrochim. Acta* **2019**, *293*, 105−115.
(28) Białek, R.; Friebe, V.; Ruff, A.; Jones, M. R.; Frese, R.; Gibasiewicz, K. In Situ Spectroelectrochemical Investigation of a Biophotoelectrode Based on Photoreaction Centers Embedded in a Redox Hydrogel. *Electrochim. Acta* **2020**, *330*, No. 135190.
(29) Gibasiewicz, K.; Pajzderska, M.; Dobek, A.; Karolczak, J.; Burdziński, G.; Brettel, K.; Jones, M. R. Analysis of the Temperature-Dependence of P+HA− Charge Recombination in the Rhodobacter Sphaeroides Reaction Center Suggests Nanosecond Temperature-

https://dx.doi.org/10.1021/acs.jpcb.0c08714
J. Phys. Chem. B 2020, 124, 11123−11132

Independent Protein Relaxation. *Phys. Chem. Chem. Phys.* **2013**, *15*, No. 16321.
(30) Gibasiewicz, K.; Białek, R.; Pajzderska, M.; Karolczak, J.; Burdziński, G.; Jones, M. R.; Brettel, K. Weak Temperature Dependence of P + H A − Recombination in Mutant Rhodobacter Sphaeroides Reaction Centers. *Photosynth. Res.* **2016**, *128*, 243−258.
(31) Pan, J.; Saer, R.; Lin, S.; Beatty, J. T.; Woodbury, N. W. Electron Transfer in Bacterial Reaction Centers with the Photoactive Bacteriopheophytin Replaced by a Bacteriochlorophyll through Coordinating Ligand Substitution. *Biochemistry* **2016**, *55*, 4909−4918.
(32) Faries, K. M.; Dylla, N. P.; Hanson, D. K.; Holten, D.; Laible, P. D.; Kirmaier, C. Manipulating the Energetics and Rates of Electron Transfer in Rhodobacter Capsulatus Reaction Centers with Asymmetric Pigment Content. *J. Phys. Chem. B* **2017**, *121*, 6989−7004.
(33) Zabelin, A. A.; Khristin, A. M.; Shkuropatova, V. A.; Khatypov, R. A.; Shkuropatov, A. Y. Primary Electron Transfer in Rhodobacter Sphaeroides R-26 Reaction Centers under Dehydration Conditions. *Biochim. Biophys. Acta, Bioenerg.* **2020**, *1861*, No. 148238.
(34) Lanzani, G. *The Photophysics behind Photovoltaics and Photonics*; Wiley-VCH Verlag GmbH & Co. KGaA: Weinheim, Germany, 2012.
(35) Szewczyk, S.; Białek, R.; Giera, W.; Burdziński, G.; van Grondelle, R.; Gibasiewicz, K. Excitation Dynamics in Photosystem I Trapped in TiO2 Mesopores. *Photosynth. Res.* **2020**, *144*, 235−245.
(36) Kothe, T.; Plumeré, N.; Badura, A.; Nowaczyk, M. M.; Guschin, D. A.; Rögner, M.; Schuhmann, W. Combination of A Photosystem 1-Based Photocathode and a Photosystem 2-Based Photoanode to a Z-Scheme Mimic for Biophotovoltaic Applications. *Angew. Chem., Int. Ed.* **2013**, *52*, 14233−14236.
(37) Kothe, T.; Pöller, S.; Zhao, F.; Fortgang, P.; Rögner, M.; Schuhmann, W.; Plumeré, N. Engineered Electron-Transfer Chain in Photosystem 1 Based Photocathodes Outperforms Electron-Transfer Rates in Natural Photosynthesis. *Chem. - Eur. J.* **2014**, *20*, 11029−11034.
(38) Zhao, F.; Wang, P.; Ruff, A.; Hartmann, V.; Zacarias, S.; Pereira, I. A. C.; Nowaczyk, M. M.; Rögner, M.; Conzuelo, F.; Schuhmann, W. A Photosystem i Monolayer with Anisotropic Electron Flow Enables Z-Scheme like Photosynthetic Water Splitting. *Energy Environ. Sci.* **2019**, *12*, 3133−3143.
(39) Badura, A.; Guschin, D.; Esper, B.; Kothe, T.; Neugebauer, S.; Schuhmann, W.; Rögner, M. Photo-Induced Electron Transfer Between Photosystem 2 via Cross-Linked Redox Hydrogels. *Electroanalysis* **2008**, *20*, 1043−1047.
(40) Sokol, K. P.; Mersch, D.; Hartmann, V.; Zhang, J. Z.; Nowaczyk, M. M.; Rögner, M.; Ruff, A.; Schuhmann, W.; Plumeré, N.; Reisner, E. Rational Wiring of Photosystem II to Hierarchical Indium Tin Oxide Electrodes Using Redox Polymers. *Energy Environ. Sci.* **2016**, *9*, 3698−3709.
(41) Sokol, K. P.; Robinson, W. E.; Warnan, J.; Kornienko, N.; Nowaczyk, M. M.; Ruff, A.; Zhang, J. Z.; Reisner, E. Bias-Free Photoelectrochemical Water Splitting with Photosystem II on a Dye-Sensitized Photoanode Wired to Hydrogenase. *Nat. Energy* **2018**, *3*, 944−951.
(42) Pishko, M. V.; Katakis, I.; Lindquist, S. -E.; Ye, L.; Gregg, B. A.; Heller, A. Direct Electrical Communication between Graphite Electrodes and Surface Adsorbed Glucose Oxidase/Redox Polymer Complexes. *Angew. Chem., Int. Ed.* **1990**, *29*, 82−84.
(43) Heller, A. Electrical Connection of Enzyme Redox Centers to Electrodes. *J. Phys. Chem. A* **1992**, *96*, 3579−3587.
(44) Teanphonkrang, S.; Janke, S.; Chaiyen, P.; Sucharitakul, J.; Suginta, W.; Khunkaewla, P.; Schuhmann, W.; Ruff, A.; Schulte, A. Tuned Amperometric Detection of Reduced β-Nicotinamide Adenine Dinucleotide by Allosteric Modulation of the Reductase Component of the p -Hydroxyphenylacetate Hydroxylase Immobilized within a Redox Polymer. *Anal. Chem.* **2018**, *90*, 5703−5711.
(45) Janoschka, T.; Martin, N.; Martin, U.; Friebe, C.; Morgenstern, S.; Hiller, H.; Hager, M. D.; Schubert, U. S. An Aqueous, Polymer-Based Redox-Flow Battery Using Non-Corrosive, Safe, and Low-Cost Materials. *Nature* **2015**, *527*, 78−81.
(46) Swainsbury, D. J. K.; Friebe, V. M.; Frese, R. N.; Jones, M. R. Evaluation of a Biohybrid Photoelectrochemical Cell Employing the Purple Bacterial Reaction Centre as a Biosensor for Herbicides. *Biosens. Bioelectron.* **2014**, *58*, 172−178.
(47) Liu, J.; Friebe, V. M.; Frese, R. N.; Jones, M. R. Polychromatic Solar Energy Conversion in Pigment-Protein Chimeras That Unite the Two Kingdoms of (Bacterio)Chlorophyll-Based Photosynthesis. *Nat. Commun.* **2020**, *11*, No. 1542.
(48) Conzuelo, F.; Marković, N.; Ruff, A.; Schuhmann, W. The Open Circuit Voltage in Biofuel Cells: Nernstian Shift in Pseudocapacitive Electrodes. *Angew. Chem., Int. Ed.* **2018**, *57*, 13681−13685.
(49) Alsaoub, S.; Ruff, A.; Conzuelo, F.; Ventosa, E.; Ludwig, R.; Shleev, S.; Schuhmann, W. An Intrinsic Self-Charging Biosupercapacitor Comprised of a High-Potential Bioanode and a Low-Potential Biocathode. *Chempluschem* **2017**, *82*, 576−583.
(50) Owen, T. *Fundamentals of Modern UV-Visible Spectroscopy*; Agilent Technologies: Germany, 2000.
(51) Jones, E.; Travis, O.; Peterson, P. SciPy: Open Source Scientific Tools for Python. http://www.scipy.org/ (accessed Jan 28 , 2019).
(52) van Stokkum, I. H. M.; Larsen, D. S.; van Grondelle, R. Global and Target Analysis of Time-Resolved Spectra. *Biochim. Biophys. Acta, Bioenerg.* **2004**, *1657*, 82−104.
(53) Snellenburg, J. J.; Laptenok, S. P.; Seger, R.; Mullen, K. M.; van Stokkum, I. H. M. Glotaran: A Java-Based Graphical User Interface for the R Package TIMP. *J. Stat. Software* **2012**, *49*, 1−2.
(54) Gibasiewicz, K.; Pajzderska, M.; Dobek, A.; Brettel, K.; Jones, M. R. Analysis of the Kinetics of P + H A − Recombination in Membrane-Embedded Wild-Type and Mutant Rhodobacter Sphaeroides Reaction Centers between 298 and 77 K Indicates That the Adjacent Negatively Charged Q A Ubiquinone Modulates the Free Energy of P + H A. *J. Phys. Chem. B* **2013**, *117*, 11112−11123.
(55) Gibasiewicz, K.; Pajzderska, M.; Ziółek, M.; Karolczak, J.; Dobek, A. Internal Electrostatic Control of the Primary Charge Separation and Recombination in Reaction Centers from Rhodobacter Sphaeroides Revealed by Femtosecond Transient Absorption. *J. Phys. Chem. B* **2009**, *113*, 11023−11031.
(56) Mandal, S.; Carey, A.-M.; Locsin, J.; Gao, B.-R.; Williams, J. C.; Allen, J. P.; Lin, S.; Woodbury, N. W. Mechanism of Triplet Energy Transfer in Photosynthetic Bacterial Reaction Centers. *J. Phys. Chem. B* **2017**, *121*, 6499−6510.
(57) Białek, R.; Burdziński, G.; Jones, M. R.; Gibasiewicz, K. Bacteriopheophytin Triplet State in Rhodobacter Sphaeroides Reaction Centers. *Photosynth. Res.* **2016**, *129*, 205−216.
(58) Friebe, V. M.; Swainsbury, D. J. K.; Fyfe, P. K.; van der Heijden, W.; Jones, M. R.; Frese, R. N. On the Mechanism of Ubiquinone Mediated Photocurrent Generation by a Reaction Center Based Photocathode. *Biochim. Biophys. Acta, Bioenerg.* **2016**, *1857*, 1925−1934.
(59) Wraight, C. A.; Gunner, M. R. The Acceptor Quinones of Purple Photosynthetic Bacteria — Structure and Spectroscopy. In *The Purple Phototrophic Bacteria*; Neil Hunter, C.; Daldal, F.; Thurnauer, M. C.; Beatty, J. T., Eds.; Springer, 2009; pp 379−405.
(60) Overfield, R. E.; Wraight, C. A. Oxidation of Cytochromes c and C2 by Bacterial Photosynthetic Reaction Centers in Phospholipid Vesicles. 1. Studies with Neutral Membranes. *Biochemistry* **1980**, *19*, 3322−3327.
(61) Ermler, U.; Fritzsch, G.; Buchanan, S. K.; Michel, H. Structure of the Photosynthetic Reaction Centre from Rhodobacter Sphaeroides at 2.65 å Resolution: Cofactors and Protein-Cofactor Interactions. *Structure* **1994**, *2*, 925−936.
(62) Dolinsky, T. J.; Nielsen, J. E.; McCammon, J. A.; Baker, N. A. PDB2PQR: An Automated Pipeline for the Setup of Poisson-Boltzmann Electrostatics Calculations. *Nucleic Acids Res.* **2004**, *32*, W665−W667.
(63) Baker, N. A.; Sept, D.; Joseph, S.; Holst, M. J.; McCammon, J. A. Electrostatics of Nanosystems: Application to Microtubules and the Ribosome. *Proc. Natl. Acad. Sci. U.S.A.* **2001**, *98*, 10037−10041.

https://dx.doi.org/10.1021/acs.jpcb.0c08714
J. Phys. Chem. B 2020, 124, 11123−11132